

# PCCP

Accepted Manuscript



This is an *Accepted Manuscript*, which has been through the Royal Society of Chemistry peer review process and has been accepted for publication.

*Accepted Manuscripts* are published online shortly after acceptance, before technical editing, formatting and proof reading. Using this free service, authors can make their results available to the community, in citable form, before we publish the edited article. We will replace this *Accepted Manuscript* with the edited and formatted *Advance Article* as soon as it is available.

You can find more information about *Accepted Manuscripts* in the [Information for Authors](#).

Please note that technical editing may introduce minor changes to the text and/or graphics, which may alter content. The journal's standard [Terms & Conditions](#) and the [Ethical guidelines](#) still apply. In no event shall the Royal Society of Chemistry be held responsible for any errors or omissions in this *Accepted Manuscript* or any consequences arising from the use of any information it contains.

## Temperature dependent nanomorphology–performance relations in binary iridium complex blend films for organic light emitting diodes

Young-Tae Kim<sup>†,a</sup>, Young-Hoon Kim<sup>†,a</sup>, Jae-Bok Seol<sup>a,b,\*</sup>, Tae-Woo Lee<sup>a</sup>, Chan-Gyung Park<sup>a,b</sup>

<sup>a</sup>*Department of Material Science and Engineering, Pohang University of Science and Technology (POSTECH), Pohang 790-784, South Korea*

<sup>b</sup>*National Institute for Nanomaterials Technology (NINT), POSTECH, Pohang 790-784, South Korea*

### Abstract

Understanding the mechanism responsible for temperature dependent performances of emitting layers is essential for developing advanced phosphorescent organic light emitting diodes. We described the morphological evolution occurring in the PVK:Ir(ppy)<sub>3</sub> binary blend films with respect to thermal annealing up to 300 °C by coupling atomic force microscopy and transmission electron microscopy. In particular, in-situ temperature dependent experimental characterization was performed to directly determine the overall sequence of morphological evolution occurring in the films. Thermally annealed device at 200 °C exhibits a noticeable enhancement in the performances, compared to the devices in as-processed state and to the devices annealed at 300 °C. Our approaches reveal that the Ir(ppy)<sub>3</sub> molecules with needle-like structure in the as-processed state were aggregated and thus diffused into PVK without their morphological change at the temperature regime between 150 °C and 200 °C. Moreover, both network-like and droplet patterns existed in the devices annealed at 300 °C which was beyond glass temperature of PVK, leading to a profound increase in the surface roughness. The observed pattern formation is discussed in terms of viscoelastic phase separation. Based on our experimental findings, we propose that the performances of devices are significantly controlled by the diffusion of dopant molecules and the morphological evolution of host materials in binary blend systems.

Keywords: Organic light emitting diodes; PVK:Ir(ppy)<sub>3</sub> binary blends; Thermal annealing; Morphological evolution; In-situ temperature dependent TEM

<sup>†</sup>Authors contributed equally to this work.

\*Corresponding author: Tel: +82 54 279 0220; e-mail: jb\_seol@postech.ac.kr (Jae-Bok Seol)

## Introduction

Organic light emitting diodes (OLEDs) have progressively received great attentions for flat-panel display and illumination light source applications [1]. Pronounced manufacture of emitting layers in the OLEDs with superior electrical properties has so far been achieved through vacuum-deposition and solution-process. First, the vacuum-deposition process has been commercially performed as it promotes the efficiency of the devices. On the other hand, the solution-processing has been introduced as promising emerging manufacturing process even though it provides the reduced efficiency of devices compared to the former. This is due to a fact that the latter offers numerous feasible advantages such as inexpensive process, low material waste, and large-scale manufacturing for lightweight flexible devices [2–4]. For the enhanced strategy of solution-processing with better performances, various techniques have systematically been considered via tailoring an optimal morphology beneficial for both charge transport and exciton confinement [5]. For instance, the chemical and electrical properties of polymer-based electroluminescent devices could be controlled by modifying the synthetic chemistry techniques of emitting materials. Moreover, a more pronounced enhancement in the performances of devices was acquired by means of varying with processing conditions such as solvent type, annealing treatment, and spin-coating speed during a fabrication [6–9]. Among these strategies, thermal annealing treatment has played important role on easily controlling device performance as discussed previously [10–16]. The general interpretation of such annealing effects on the device is that an enhancement in interfacial bonding between substrate and organic layers promotes the surface planarity of organic films. As a result, an electron-hole recombination is promoted. To better understand such a mechanism, atomic force microscopy (AFM) has been widely performed to reveal the correlations between surface planarity and device performance with respect to thermal annealing treatment of OLEDs [17–21].

Besides the surface planarity of organic films, the distribution of guest and host components in emitting layer during a thermal annealing are also the governing microstructure components for developing efficient solution-processed OLEDs. Previous studies suggested that the aggregation of guest molecules yields the loss of luminescence efficiency due to their concentration quenching [22–24]. More recently, it was dedicated that homogeneously distributed guest molecule in host matrix

was beneficial for an efficient energy transfer from host to guest molecules [25–26]. Consequently, an electron–hole recombination associated with the nanomorphology and distribution of guest molecule is important in an enhancement in the performances of solution–processed OLEDs. However, direct experimental evidence on understanding of the microstructure components responsible for temperature–dependent performances of the organic-based devices is still lacking. To date, it has been a great challenge to tackle this issue due to a lack of in–situ temperature–dependent experimental characterization. Therefore, a specific challenge for in–situ heating transmission electron microscopy (TEM) approach lies in characterizing the overall sequence of microstructural evolution occurring in emitting layer consisting of guest and host materials.

More specific, this study aims at elucidating the pronounced correlations between temperature–dependent device performance and annealing–induced phenomena within the emitting layers. Here, we studied the Tris(2–phenylpyridine) iridium(III) ( $\text{Ir}(\text{ppy})_3$ ) blended into poly(N–vinyl carbazole) (namely PVK: $\text{Ir}(\text{ppy})_3$  binary blend films) used for green emitting OLEDs [30–32]. Thus, we subject these materials to experimental approaches from the in–situ heating to the ex–situ annealing for placing a particular attention on the morphological change of both PVK polymer and  $\text{Ir}(\text{ppy})_3$  molecule as well as on the associated concentration gradient of iridium. Based on our observation, an insight into the phase separation in polymer blend film and into the diffusion of guest molecules during thermal annealing will give us better understanding of the relevant nanomorphology–performance correlations in phosphorescent OLEDs.

## Experimental

PVK: $\text{Ir}(\text{ppy})_3$  binary blend based OLEDs were fabricated through solution-processing. Indium tin oxide (ITO) coated on glass was used as a substrate material. The surface of glass was cleaned and treated through following three steps; sonication in acetone and 2-isopropanol (IPA) for 15 min, followed by UV–ozone for 10 min. Next, a hole injection layer (HIL) with a thickness of 40 nm was deposited by spin–coating. In particular, we used the HIL composed with poly(3,4–ethylene dioxythiophene) : polystyrene (sulfonic acid) : tetrafluoroethylene-perfluoro-3,6-dioxo-4-methyl-7-octene-sulfonic acid copolymer (called PEDOT:PSS:PFI) for better electron–hole recombination [32–35]. Subsequently, it was transferred into the glove box after baking at 150 °C for 30 min prior to fabrication of emitting layer, for eliminating the solvent in HIL. After baking, PVK:  $\text{Ir}(\text{ppy})_3$  blend diluted in the chlorobenzene as a mixture with PVK:  $\text{Ir}(\text{ppy})_3$  ratio of 10:1.5 was spin–coated at 2000 rpm for 90 sec. In this study, PVK:  $\text{Ir}(\text{ppy})_3$  films with a thickness of 50 nm were deposited on the

HIL. They were thermally annealed at 80, 150, 200, 250, and 300 °C for 60 min. After annealing, 1,3,5-tris(1-phenyl-1H-benzimidazol-2-yl)benzene (TPBI) with a thickness of 50 nm, 1-nm thick LiF, and 100-nm thick Al cathode layers were progressively deposited in the vacuum condition of  $<10^{-7}$  Torr for fabrication of phosphorescent OLEDs. The thickness of the fabricated devices was determined through TEM characterization. Fig. 1 shows the chemical structures of the binary blend components used in this study, TEM image of the overall stacking structure of devices, and the corresponding energy level diagrams.

The electrical properties of as-processed and thermally annealed devices were determined by their current density–voltage (J–V) characteristics with a sourcemeter (Keithley 236). The voltage (V)–luminance (L) characteristics were measured by a spectroradiometer (Minolta CS2000).

Samples for TEM observation were prepared by a floating method, prior to the deposition of electron-injection layer (EIL) and Al cathode layers. After fully dissolving the HIL of PEDOT:PSS:PFI in pure water, the PVK:Ir(ppy)<sub>3</sub> films floating on water were picked up in terms of TEM mesh grids. Morphological evolution in PVK:Ir(ppy)<sub>3</sub> binary blends occurring during a thermal annealing was characterized by TEM (JEM 2010F) at an acceleration voltage of 200 kV. For measuring the iridium concentrations, energy dispersive X-ray spectrometry (EDS) of aberration-corrected scanning TEM (Cs-STEM) equipped with high angle annular dark field (HAADF) detector was performed. In addition, in-situ temperature dependent TEM approach was conducted with a heating specimen holder (GATAN). Using this approach, the nanomorphology of PVK:Ir(ppy)<sub>3</sub> films was systematically observed with respect to annealing temperature ranging from room temperature to 300 °C. In particular, we observed time-dependent pattern evolution in the polymer at 300 °C for 300 s. When in-situ heating TEM experiments, temperature was progressively controlled by heating with a step of 10 °C for every 1 min. Surface roughness of PVK:Ir(ppy)<sub>3</sub> binary blends was determined by AFM height and amplitude maps obtained in tapping mode.

## Results and discussion

The performance of the present devices varies significantly with the applied annealing temperature ranging from room temperature to 300 °C. The enhanced current density is present in the device of Ir(ppy)<sub>3</sub> doped PVK emitting layer annealed at 200 °C, and the device with emitting layers annealed at 300 °C represents a substantial leakage current (Fig. 2a). The devices including Ir(ppy)<sub>3</sub> doped PVK emitting layer in as-processed state and annealed at 200 °C displayed electro-luminescence (EL) peak at 512 nm corresponding to Ir(ppy)<sub>3</sub> molecules showing a clear green emission (Fig. 2b). This implies

that efficient energy transfer from polymer host PVK to Ir(ppy)<sub>3</sub> dopant molecules occurs for as-processed devices and annealed devices at 200 °C. On the other hand, the thermally annealed devices at 300 °C showed emission peak at 412 nm arising from PVK. It reveals that energy transfer from PVK to Ir(ppy)<sub>3</sub> was prohibited by annealing at 300 °C, and thus emitted only blue light from PVK. The measured current efficiency and luminance of the devices annealed at 200 °C showed ~14.6 cd/A and ~5000 cd/m<sup>2</sup>, while ~3.8 cd/A and ~360 cd/m<sup>2</sup> for the devices in as-processed state and ~0.14 cd/A and ~130 cd/m<sup>2</sup> for annealed at 300 °C, respectively (Figs. 2b and 2c). A more propound enhancement in the efficiency and luminance of devices annealed at 200 °C is likely to be responsible for an increase in the radiative electron-hole recombination. This means that better energy transfer from PVK to Ir(ppy)<sub>3</sub> and lower intermolecular quenching between Ir(ppy)<sub>3</sub> molecules can be achieved. Therefore, we found that the performances of PVK:Ir(ppy)<sub>3</sub> binary blend containing OLEDs significantly depend on the temperature ranging from room temperature to 300 °C. Moreover, this observation is analogous to the previous studies that an appropriate thermal annealing of PVK:Ir(ppy)<sub>3</sub> films is favorable for better energy transfer of the solution-processed OLEDs.

So as to reveal the relations between temperature-dependent performances and nanostructure of PVK:Ir(ppy)<sub>3</sub> binary blend films, in-situ temperature dependent TEM experiments were performed as shown in Fig. 3. This approach enables us to directly provide the overall sequence of morphological evolution occurring in the film during thermal heating. Prior to annealing treatment (called as-processed state), two-dimensional aggregation is homogeneously distributed in polymer matrix (PVK), showing the needle-like features with a high aspect ratio (a length of 1~2 μm, a width of 30~40 nm) as shown in Fig. 3a. The needles appear to be darker than that of PVK matrix in the TEM images. It has been generally known that when using the bright-field mode of TEM, the contrast of regions with a higher atomic number appears to be darker due to larger electron scattering. Taking into account a higher atomic number of iridium than components of PVK, the needle-type aggregations with darker contrast are likely to be Ir(ppy)<sub>3</sub> molecules. With increasing temperature up to 150 °C, the contrast at the corner of needle-type Ir(ppy)<sub>3</sub> aggregations becomes brighter gradually compared to PVK. Namely, the bright and dark regions of needle-type Ir(ppy)<sub>3</sub> molecules can be clearly distinguished as marked with the arrows shown in Fig. 3c. This indicates that a local contrast variation of Ir(ppy)<sub>3</sub> needles is promoted by thermal annealing, but within a limited temperature regime. Nevertheless, thermal annealing at 150 °C did not induce any important morphological evolution of the needles. The measured morphological parameters, such as width and length of needles, were constant. Around a higher temperature of 200 °C, the contrast of Ir(ppy)<sub>3</sub> needles becomes fully bright as shown in Fig. 3d. At 250 °C which was above the glass-transition temperature (T<sub>g</sub>) of PVK in the present case, the interface between Ir(ppy)<sub>3</sub> molecules and host materials is blurred

and thus the needles disappear gradually. At the temperature of 300 °C, the network-like patterns are present in the earlier state (Fig. 3f) and then the circular particles are observed with a longer time (Figs. 3g and 3h). This means that during annealing of 300 °C the network structure eventually transforms into the droplet patterns or circular particles. The observed pattern evolution in the devices annealed at 300 °C agrees with previous experimental results and numerical simulation of polymer solutions [36]. Following this concept, we propose that thermal annealing above the  $T_g$  can make polymer materials exhibit a fluid-like behavior and hence the movement of the polymer chains is activated. As a result, the polymer chains above the  $T_g$  can become mobile and form the network structures as shown in Figs. 3(f)–3(h). The contrast of polymer regions is temporally getting darker with time, which means host PVK polymer aggregation becomes dense. After a while, the thin parts of the polymer aggregates are elongated and droplet structure can be formed due to the elastic force balance instead of interfacial tension (Fig. 3h) [36]. Based on our TEM results and those found in the literature, we consider that the observed spherical particles found in the films annealed at 300 °C are likely to be attributed to a polymer phase separation of PVK during thermal annealing. And hence, the energy transfer from host to guest could not occur efficiently due to the phase separation or the aggregation of host PVK, resulting in the noticeable degradation of current efficiency and luminance for the devices annealed at 300 °C. Using in-situ temperature dependent TEM characterization, we found that the morphological or pattern evolution is an important factor contributing to device performances of solution-processed PVK:Ir(ppy)<sub>3</sub> binary blend films. Further detailed information of circular particles observed at the devices annealed at 300 °C is discussed in next section.

More specific attention is paid on the origin of needle-type aggregations observed in the as-processed devices, and on the local contrast changes in thermally annealed devices at 150 °C as well as on the circular particles in the device annealed at 300 °C. To resolve these issues, the EDS and HAADF techniques of ex-situ (S)TEM analysis were performed. EDS results revealed that the concentration of iridium atoms along the direction (marked with the arrows) across the interfaces between needles and PVK significantly varies with the applied annealing temperature as shown in Fig. 4. In the as-processed state, two-dimensional nanostructure with needle-type morphology is visible (Fig. 4a). This is in good accordance with in-situ heating TEM experiments shown in Fig. 2a. Generally, the contrast shown in HAADF image is reversed to bright-field mode of TEM, i.e., heavier element contributes to a brighter contrast. Fig. 4b displays the corresponding EDS mapping of iridium atoms, revealing that the observed needle-like features are unambiguously Ir(ppy)<sub>3</sub> molecules. Here, the intensity-profiles of 1.977 eV corresponding to Ir-M<sub>α</sub> signals were acquired from the needle-like features. We demonstrate that the aggregation of Ir(ppy)<sub>3</sub> found in the as-processed devices introduces inefficient energy transfer and severe exciton quenching, leading to a degraded performance of the

devices (Fig. 2). The origin of needle-like features of guest molecules was systematically revealed in the earlier studies [37-39]. For instance, the needle-like aggregation of EPPTC molecules embedded in PFO film could be formed through  $\pi$ -stacking during a spin-coating process [37]. Similarly, Liu et al. [38] proved from the result of X-ray diffraction (XRD) that the  $\pi$ -stacking interaction in the solid state played an important role in highly ordered extended aggregation morphology of conjugated molecular systems. More recently, Salim et al. [39] suggested that the observation of needle-type Ir(ppy)<sub>3</sub> aggregates in ternary blend films was an indicator of the ability of Ir(ppy)<sub>3</sub> molecules to self-assemble into nanostructures even under spin-coating. Therefore, we propose that the formation of needle-like Ir(ppy)<sub>3</sub> aggregates in PVK:Ir(ppy)<sub>3</sub> binary system at room temperature (namely as-processed state) is likely to be ascribed to assemble themselves during the solvent evaporation of solution-processed OLEDs fabrication. Additionally, our TEM observation of needle-type Ir(ppy)<sub>3</sub> molecules in PVK:Ir(ppy)<sub>3</sub> binary system has not been introduced to date, except for Ir(ppy)<sub>3</sub> molecules in the P3HT, PF, and PFHP films [38-41].

High-resolution (S)TEM and HAADF images taken from the thermally annealed films at 150 °C shows a local contrast variation of Ir(ppy)<sub>3</sub> needles, which is promoted by thermal annealing (Figs. 4c and 4d). This agrees with the results acquired through in-situ heating TEM approach as shown in Fig 3c. Although the experimental pressure during in-situ heating approach is much lower compared to ex-situ thermal annealing, temperature difference of the two approaches was not efficient in this study. From this TEM observation, we found that a noticeable enhancement in the emitting efficiency of devices annealed at 200 °C (Fig. 2) is substantially attributed to the contrast changes of needle-type Ir(ppy)<sub>3</sub> aggregation (see Fig. 3c, and Figs. 4c~4d). EDS analysis revealed the origin of the contrast change observed in the needles for the thermally annealed devices. It is the concentration gradient of Ir(ppy)<sub>3</sub> molecules that occurred during thermal annealing. Clearly, the distribution of iridium atoms along the direction (marked with the arrows) across the interfaces between needles and PVK is homogeneous as represented with red line in Fig. 4f. Moreover, the Ir-M<sub>α</sub> peak of 1.977 eV and the Ir-L<sub>α</sub> peaks of 9.174 eV were strongly detected at the brighter regions in HAADF image as shown in Supplementary Information of Fig. S1. Thus, we did not detect any remarkable concentration disparity of carbon and nitrogen between matrix and needle region regardless of annealing temperature. Considering that Ir(ppy)<sub>3</sub> molecules mainly consist of carbon and nitrogen, it is plausible that the observed concentration gradient of needle-type Ir(ppy)<sub>3</sub> molecules in the devices annealed at temperature ranges between 150 °C and 200 °C is induced not by the decomposition of iridium and carbon atoms separately, but by the diffusion of Ir(ppy)<sub>3</sub> molecules themselves. This is due to thermal stability of Ir(ppy)<sub>3</sub> molecules below temperature of 300 °C [42]. Based on our results, we suggest that the origin of a pronounced enhancement in the emitting performances of solution-processed OLEDs

by up to three orders of magnitude is the diffusion of Ir(ppy)<sub>3</sub> molecules associated with an appropriate annealing temperature. Thus, we consider that an increase in the annealing temperature is likely to accelerate the mobility of needle-type Ir(ppy)<sub>3</sub> aggregates themselves, leading to the diffusion of Ir(ppy)<sub>3</sub> into the PVK with sustaining needle-like morphology. However, exact kinetics of Ir(ppy)<sub>3</sub> diffusion responsible for material transport cannot be explained from a thermodynamic point of view due to a lack of database in the literature.

As an annealing temperature increases further, the circular particles were displayed instead of the needles. The observed circular particles in the emitting layer annealed at 300 °C is an indicator of the occurrence of PVK:Ir(ppy)<sub>3</sub> pattern evolution during annealing treatment. The Ir(ppy)<sub>3</sub> molecules in the emitting layer annealed at 300 °C are well distributed into PVK matrix as shown in Fig. 4f. Here, it is worth mentioning that the measured concentration of iridium along the direction (marked with the arrows) for the annealed samples at 300 °C is remarkably reduced compared to that of the films annealed at 200 °C (red line). The measured concentration of iridium in the emitting layer was below ~0.05 at.% for 300 °C films as represented with blue line in Fig. 4f. This result indicates that the spherical particles with droplet pattern found in the films annealed at 300 °C are not Ir(ppy)<sub>3</sub> molecule aggregations, but PVK aggregation. As mentioned previously, Tanaka [36] proposed that viscoelastic phase separation should be universal to any dynamically asymmetric mixtures including polymer solutions consisted of fast and slow components, and thus viscoelastic effects significantly control the critical dynamics of polymer solutions or blends. Based on our TEM findings and those in the literature, we consider that viscoelastic phase separation is likely to be mechanism responsible for the observed time-dependent pattern evolution of polymers at 300 °C.

The concentration gradients and morphological evolution affect the surface uniformity of binary blend films as shown in Fig. 5. The surface roughness of needle-type Ir(ppy)<sub>3</sub> aggregations with a high aspect ratio was 5.25 nm in the as-processed films. Meanwhile, thermal annealing up to 200 °C introduces the enhanced surface uniformity. The measured surface roughness was 2.78 nm for the device annealed at 200 °C. With an annealing temperature increases up to 300 °C, the surface uniformity was dramatically degraded due to the presence of large spherical particles with droplet pattern on the surface. The surface roughness was estimated at 9.03 nm.

By means of coupling in-situ temperature-dependent experimental and ex-situ annealing approaches carried out in the present study, the schematics are illustrated as shown in Fig. 6. The schematic illustration can explain the overall sequence of microstructural evolution in the guest and host materials occurring during thermal annealing for PVK:Ir(ppy)<sub>3</sub> binary blend system. In the as-processed state (Fig. 6a), the needle-like aggregation (blue) of Ir(ppy)<sub>3</sub> molecules (green dots) is distributed well in the PVK polymer (brown). As an increase in the temperature, the Ir(ppy)<sub>3</sub>

molecules were diffused into PVK with sustaining their original needle-like morphology as indicated with the arrows (Fig. 6b). Subsequently, the Ir(ppy)<sub>3</sub> molecules exist in the PVK polymer as shown in Fig. 6c. At 300 °C, the binary blend film shrinks and thus the spherical particles with droplet pattern (yellow) are formed in the films resulting from the phase separation of PVK (Fig. 6d).

## Conclusions

We investigated the temperature dependent efficiency, morphological evolution and dopant distribution of PVK:Ir(ppy)<sub>3</sub> binary blend emitting films with respect to the applied annealing temperature ranging from room temperature to 300 °C through in-situ temperature dependent TEM. Further analyzes of AFM and (S)TEM-EDS confirmed the characteristics found by in-situ TEM experiments. It reveals that the diffusion of Ir(ppy)<sub>3</sub> molecules and the phase separation of polymers are important in determining the device performances of solution-processed PVK:Ir(ppy)<sub>3</sub>. The main conclusions derived from our experimental results are summarized below.

1. The efficient energy transfer from PVK to Ir(ppy)<sub>3</sub> for the as-processed state and the devices at 180 °C are visible, whereas the absence of energy transfer at annealing of 300 °C. In addition, the superior combination of efficiency and luminance is achieved for the device annealed at 200 °C, indicating a higher electron-hole recombination or better exciton confinement. As a result, the performances of PVK:Ir(ppy)<sub>3</sub> binary blend based OLEDs is significantly temperature-dependent ranging from room temperature to 300 °C.
2. At a reference state, two-dimensional nanostructure tends to form in polymer films, showing the needle-like features with a high aspect ratio. Using TEM-EDS, it is revealed that the Ir(ppy)<sub>3</sub> molecules are aggregated as needle-features in PVK:Ir(ppy)<sub>3</sub> films, which was induced by the solvent evaporation of solution-processed OLEDs fabrication.
3. During annealing at 200 °C, the chemical gradient of Ir(ppy)<sub>3</sub> molecules occurs while their original needle-type morphology formed initially in the as-processed state are sustained. In addition, we demonstrated that using a quantitative analysis across the boundaries between Ir(ppy)<sub>3</sub> aggregations and PVK matrix thermal annealing at 200 °C introduces a higher mobility of Ir(ppy)<sub>3</sub> molecules and then leads to their diffusion into the host materials. Consequently, the surface uniformity is substantially improved. Therefore, the diffusion of Ir(ppy)<sub>3</sub> molecules associated with an appropriate annealing temperature rather than the formation of their needle-like morphology is responsible for the pronounced enhancement in the emitting performance of solution-processed OLEDs.
4. The devices annealed at much higher than glass temperature of host materials exhibited the

degraded efficiency and characteristics of phosphorescent emission. The observed network-like pattern and spherical particles with droplet pattern in the films annealed at 300 °C are attributed to a polymer phase separation of PVK during annealing, leading to the pronounced degradation of device performances. Here, viscoelastic phase separation is probably the mechanism underlying pattern evolution.

Overall, thermally annealed PVK:Ir(ppy)<sub>3</sub> binary blend emitting films presented in this work show good performances of current efficiency and luminance rendering them suited for phosphorescent OLEDs. In addition, our experimental approaches proposed in this study can provide direct evidence of relevant nanomorphology-performance correlations in various polymer based OLEDs.

## Acknowledgments

This work was financially supported by the National Research Foundation of Korea (NRF) grants funded by the Korean Government (MEST) (No.2011-0020252).

## References

- [1] Tang CW and S.A.Vanslyke., *Appl. Phys. Lett.* 51, 913 (1987)
- [2] H.Wu, G.Zhou, J.Zou, C.L.Ho, W.Y.Wong, W.Yang, J.Peng and Y.Cao, *Adv. Mater.* 21, 41, 4181 (2009)
- [3] K.S.Yook, S.E.Jang, S.O.Jeon and J.Y.Lee, *Adv.Mater.* 22, 40, 4479 (2010)
- [4] .L.Duan, L.Hou, T.-W.Lee, J.Qiao, D.Zhang, G.Dong, L.Wang and Y.Qiu, *J.Mater.Chem.* 20, 6392 (2010)
- [5] J.-H.Jou, S.Kumar, A.Agrawal, T.-H.Li and S.Sahoo, *J.Mater.Chem.C*, 3, 2974 (2015)
- [6] K.M.Vaeth and C.W.Tang, *J.Appl.Phys.* 92, 3447 (2002)
- [7] K.H.Yim, W.J.Doherty, W.R.Salaneck, C.E.Murphy, R.H.Friend and J.S.Kim, *Nano Lett.* 10, 385 (2010)
- [8] S.E.Shaheen, C.J.Brabec, N.S.Sariciftci, F.Padinger, T.Fromherz and J.C.hummelen, *Appl.Phys.Lett.* 78, 841 (2001)
- [9] Y.K.Kim, S.A.Choulis, J.Nelson, D.D.C.Bradley, S.Cook and J.R.Durrant, *Appl.Phys.Lett.* 86, 063502 (2005)
- [10] S Caria, E.D.Como, M.Murgia, R.Zamboni, P,Melpiganano and V.Biondo,

- J.Phys.:Condens.Matter.18, S2139 (2006)
- [11] B.J.Chen, X.W.Sun and K.R.Sarma, Materials Science and Engineering B. 139, 192-196 (2007)
- [12] G.Baldacchini, T.Baldacchini, P.Chiacchiaretta, R.B.Pode, M.A.Vincenti and Q.-M.Wang, ECS Transactions. 16, 31, 3 (2009)
- [13] M.Thomschke, S.Hofmann, S.Olthof, M.Anderson, H.Kleemann, M.Schober, B.Lussem and K.Leo, Appl.Phys.Lett. 98, 083304 (2011)
- [14] J.Liu, T.F.Guo and Y.Yang, J.Appl.Phys. 91, 3 (2002)
- [15] J.H.Ahn, C.Wang, N.E.Widdowson, C.Pearson and M.R.Bryce, J.Appl.Phys.98, 054508 (2005)
- [16] Y.H.Niu, Q.Hou and Y.Cao, Appl. Phys. Lett. 81, 634 (2002)
- [17] M.C.Sun, J.H.Jou, W.K.Weng and Y.S.Huang, Thin Solid Films. 491, 260 (2005)
- [18] M.L.Tu, Y.K.Su, S.J.Chang, T.H.Fang, W.H.Chen and H.Yang, Jpn.J.Appl.Phys. 44,4B (2005)
- [19] G.T.Chen, S.H.Su, C.C.Hou and M.Yokoyama, Journal of The Electrochemical Society.154 5, J159 (2007)
- [20] T.-W.Lee and O.O.Park, Adv. Mater. 12, 11 (2000)
- [21] J.W.Kim, J.Y.Lee, C.W.Han, N.Y.Lee and I.J.Chung, Appl. Phys. Lett. 82, 24 (2003)
- [22] Y.Kawamura, J.Brooks, J.J.Brown, H.Sasabe and C.Adachi, PRL. 96, 017404 (2006)
- [23] J.R.Gong, L.J.Wan, S.B.Lei, and C.L.Bai, J.Phys.Chem.B,109, 1675 (2005)
- [24] W.J.Shi, J.Barber, and Y.Zhao, J.Phys.Chem.B, 117, 3976 (2013)
- [25] J.H.Jou, W.B.Wang, S.Z.Chen, J.J.Shyue, M.F.Hsu, C.W.Lin, S.M.Shen, C.J.Wang, C.P.Liu, C.T.Chen, M.F.Wu and S.W.Liu, J.Mater.Chem. 20, 8411 (2010)
- [26] B.Minaev, G.Baryshnikov, H.Agren, Phys.Chem.Chem.Phys., 16, 1719 (2014)
- [27] X.Yang, J.Loos, S.C.Veenstra, W.J.H.Verhees, M.M.Wienk, J.M.Kroon, M.A.J.Michels, and R.A.J.Janssen, Nano Lett, 5, 4, 579 (2005)
- [28] A.Swinnen, I.Haeldermans, M.V.Ven, J.D'Haen, G.Vanhoyland, S.Aresu, M.D'Olieslaeger, and J.Manca, Adv.Funct. Mater, 16, 760 (2006)
- [29] X.-T.Hao, L.M.Hirvonen and T.A.Smith, Methods Appl.Fluoresc, 1, 015004 (2013)
- [30] C.L.Lee, K.B.Lee, J.J.Kim, Appl. Phys. Lett. 77, 2280 (2000)
- [31] A.Bruno, A.D.G.D.Mauro, G.Nenna, M.G.Maglione, S.A.Haque, C.Minarini, Journal of Photonics for Energy. 3, 033599 (2013)
- [32] M.-R.Choi, T.-H.Han, K.-G.Lim, S.-H.Woo, D.H.Huh, and T.-W.Lee, Angew.Chem.Int.Ed, 50, 6274 (2011)
- [33] T.-H.Han, Y.B.Lee, M.-R.Choi, S.-H.Woo, S.-H.Bae, B.H.Hong, J.-H.Ahn, T.-W.Lee, Nature photon, 6, 105 (2012)
- [34] T.-W. Lee, Y.Chung, O.Kwon, J.-J.Park, Adv. Funct. Mater. 17, 390 (2007)

- [35] Y.-H.Kim, H.Cho, J. H.Heo, T.-S.Kim, N.Myoung, C.-L.Lee, S.H.Lim, T.-W.Lee, *Adv. Mater.* 27, 7, (2015)
- [36] H.Tanaka and T.Araki, *Chemical Engineering Science.* 61, 2108 (2006)
- [37] X.Zhang, F.Dou and H.Liu, *Journal of Polymer Science: Part B: Polymer Physics.* 51, 749 (2013)
- [38] Y. Liu, G. Zhan, X. Zhong, Y. Yu and W. Gan, *Liquid Crystals.* 38, 995 (2011)
- [39] T.Salim, J.Y.Lek, B.Brauer, D.Fichou and Y.M.Lam, *Phys. Chem. Chem. Phys.* 16, 23829 (2014)
- [40] F.C.Chen, S.C.Chang, G.He, S.Pyo, Y.Yang, M.Kurotaki and J.Kido, *Journal of Polymer Science: Part B: Polymer Physics.* 41, 2681 (2003)
- [41] Y.Y.Noh, C.L.Lee and J.J.Kim, *J. Chem. Phys.* 118, 6, 2853 (2003)
- [42] N.R.Jung, E.J.Lee, J.H.Kim, H.G.Park, K.M.Park, and Y.J.Kang, *Bull.Korean Chem.Soc.* 33, 1, 183 (2012)

### Figure captions:

**Fig. 1.** (a) Chemical structures of the binary blend components, i.e. guest Ir(ppy)<sub>3</sub> and host PVK materials, (b) TEM image showing the stacking structure of OLED device containing PVK:Ir(ppy)<sub>3</sub> binary blend films, and (c) energy level diagram of the device fabricated in the present work.

**Fig. 2.** Device performances of PVK:Ir(ppy)<sub>3</sub> films with respect to thermal annealing: (a) current density, (b) EL spectra, (c) current efficiency, and (d) luminance. The blank rectangles, circles, and triangles represent the as-processed state, annealed at 200 °C and 300 °C, respectively.

**Fig. 3.** Bright-field images observed by in-situ temperature dependent TEM experiments ranging from room temperature to 300 °C: (a) as-processed PVK:Ir(ppy)<sub>3</sub> binary blend film, (b) 100 °C, (c) 150 °C, (d) 200 °C, (e) 250 °C, and (f) 300 °C, respectively. (g) and (f) The time-dependent pattern evolution occurring at 300 °C. Note that the local contrast changes of the needle-like features are shown within the limited temperature regime as marked with the arrows.

**Fig. 4.** (a) HAADF-STEM image taken from as-processed PVK:Ir(ppy)<sub>3</sub> binary blend films and (b) the corresponding enlarged EDS elemental map of Ir (M<sub>α</sub>). (c) The high-resolution (S)TEM image of the film annealed at 150 °C. HAADF-STEM images of thermally annealed at (d) 150 °C and (e) 300 °C, respectively. (f) The corresponding 1-D concentration profiles of Ir along the direction (marked

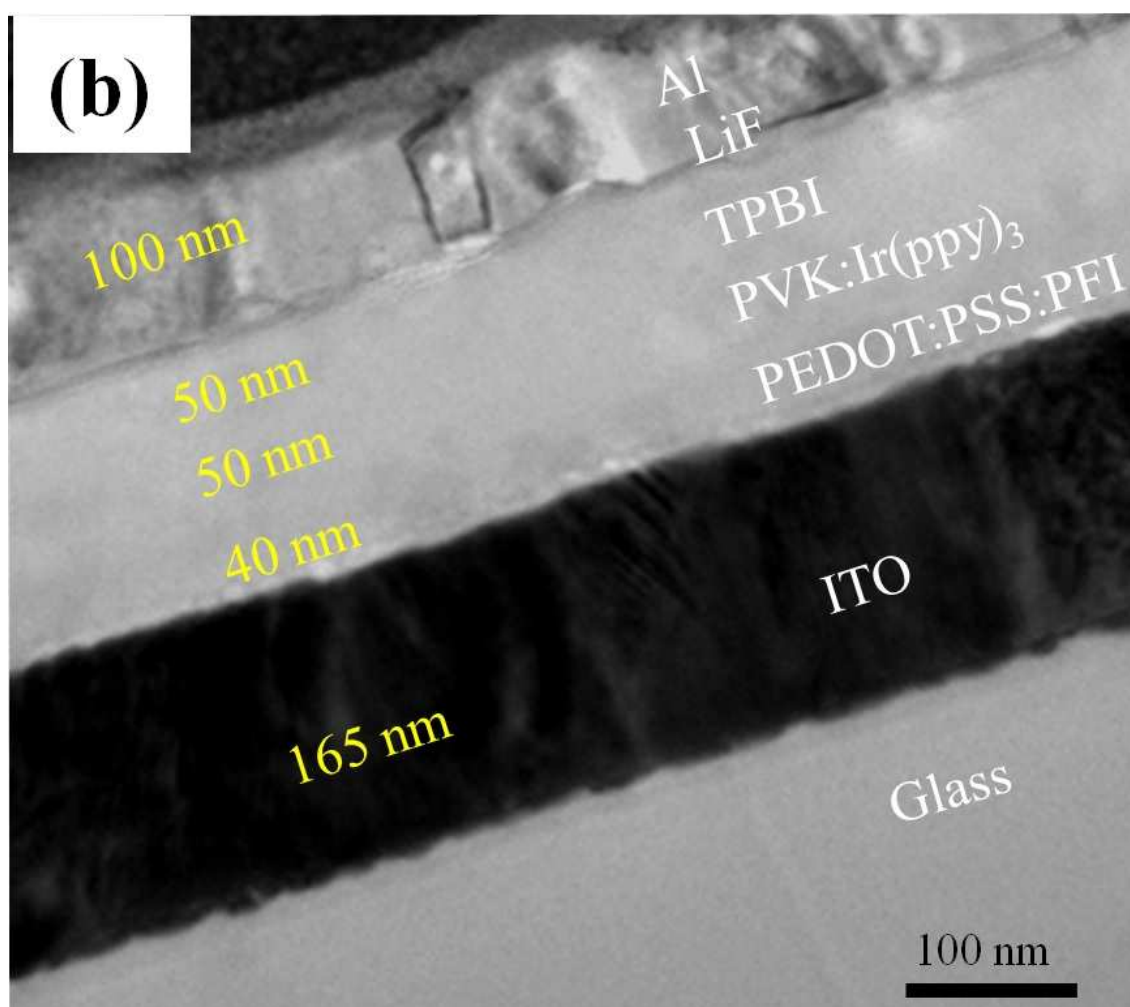
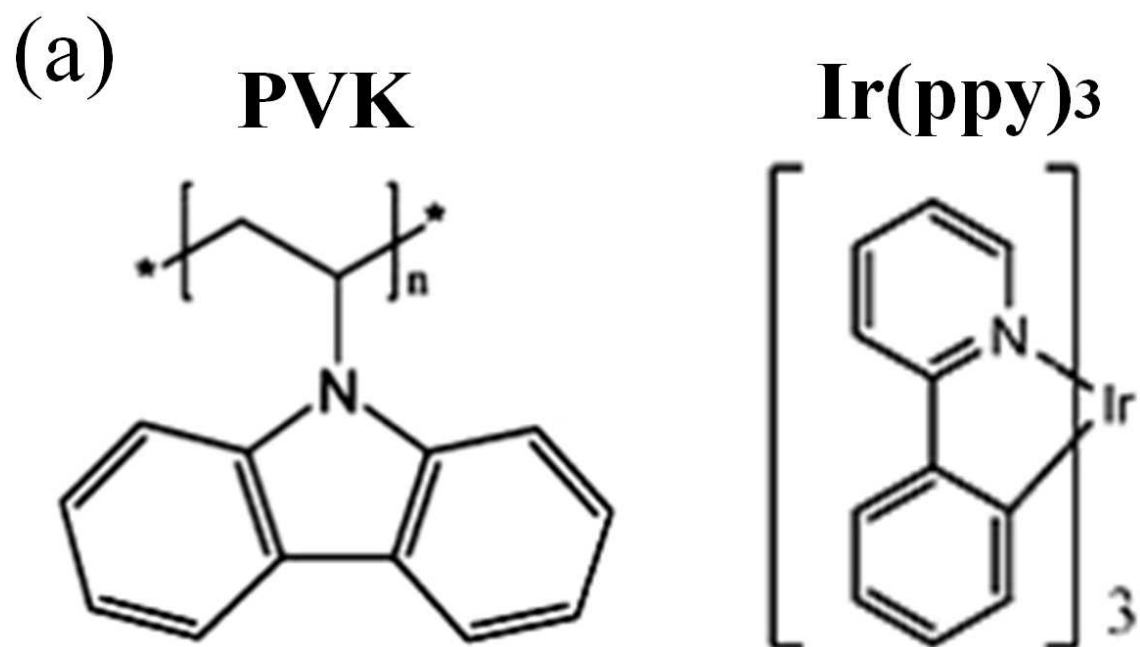
with the arrows taken from ROI) across the interfaces between needles and PVK. The rectangles, circles, and triangles represent the as-processed state, annealed at 150 °C and 300 °C, respectively.

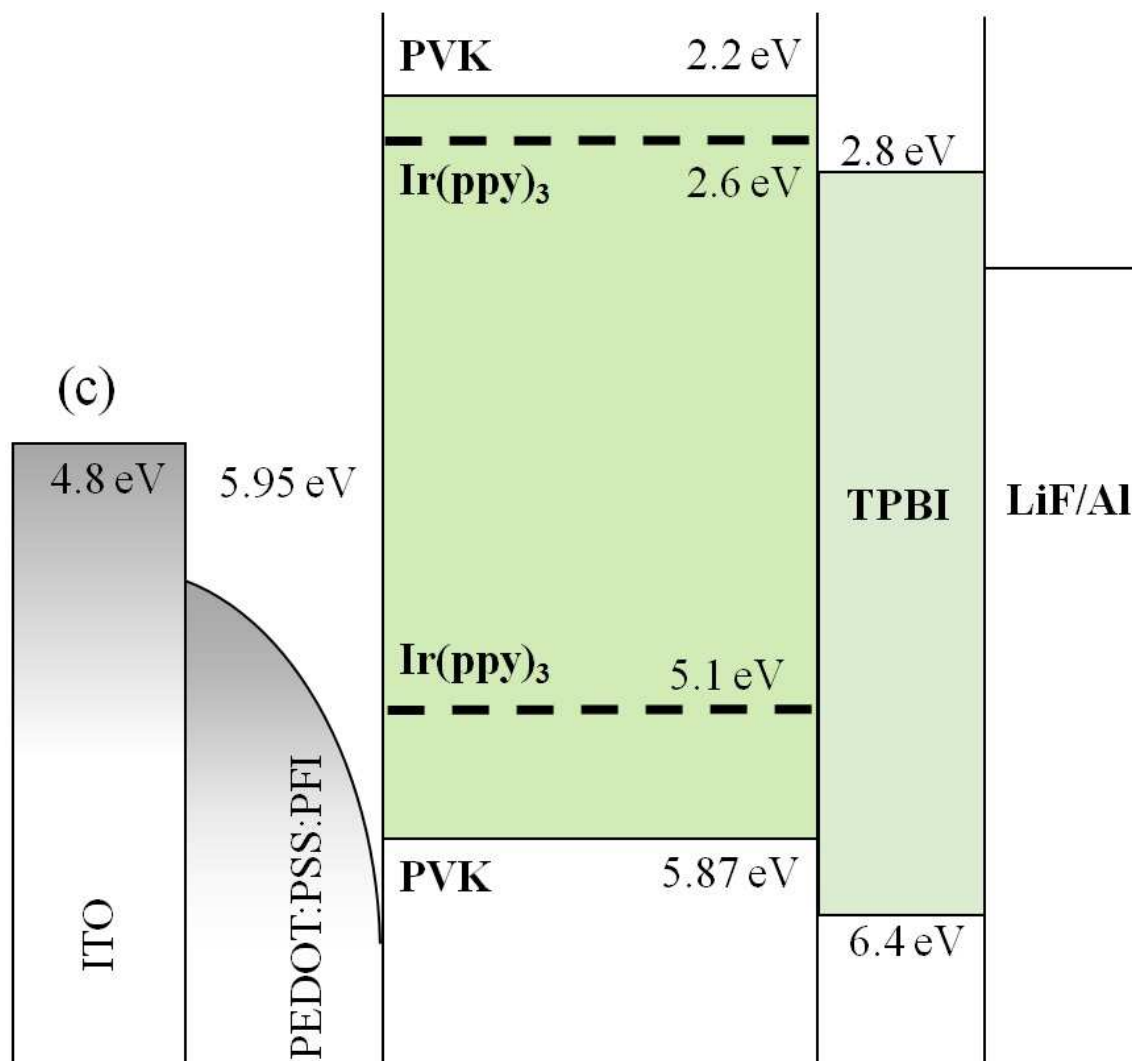
**Fig. 5.** Tapping mode AFM height images of (a) as-processed PVK:Ir(ppy)<sub>3</sub> binary blend films, and thermally annealed films at (b) 150 °C and (c) 300 °C, respectively.

**Fig. 6.** Schematic illustrations showing the overall sequence of microstructural evolution occurring in thermally annealed PVK:Ir(ppy)<sub>3</sub> binary blend system. The green dots, blue needles, and yellow circles represent Ir(ppy)<sub>3</sub>, aggregation of Ir(ppy)<sub>3</sub> molecules, and droplet pattern of PVK, respectively. Note that at 300 °C the binary blend film shrinks, leading to a reduction of its volume.

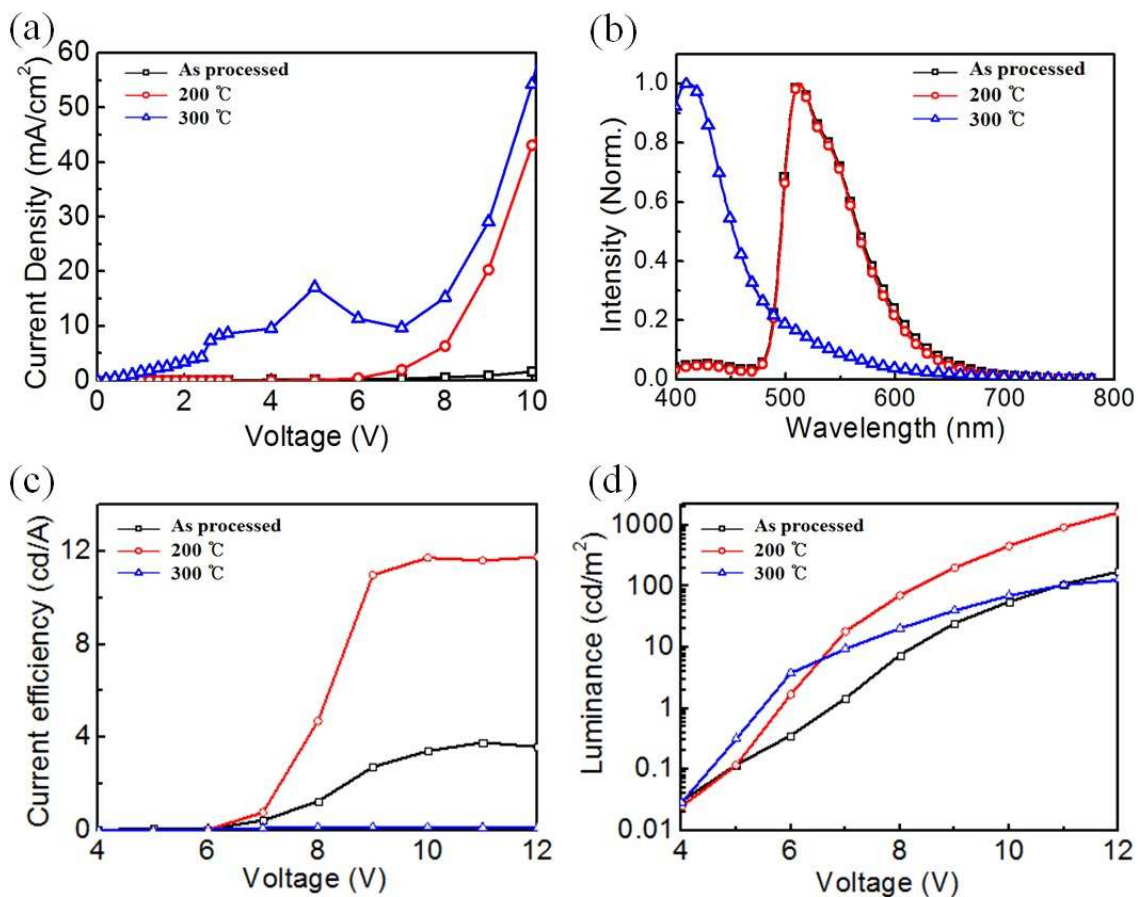
## Supplementary Information

**Fig. S1.** (S)TEM-HAADF image taken from a thermally annealed PVK:Ir(ppy)<sub>3</sub> at 150 °C showing the local contrast change of the needle-like features and the corresponding EDS results acquired from (a) PVK, (b) and (c) needle-like features, respectively.

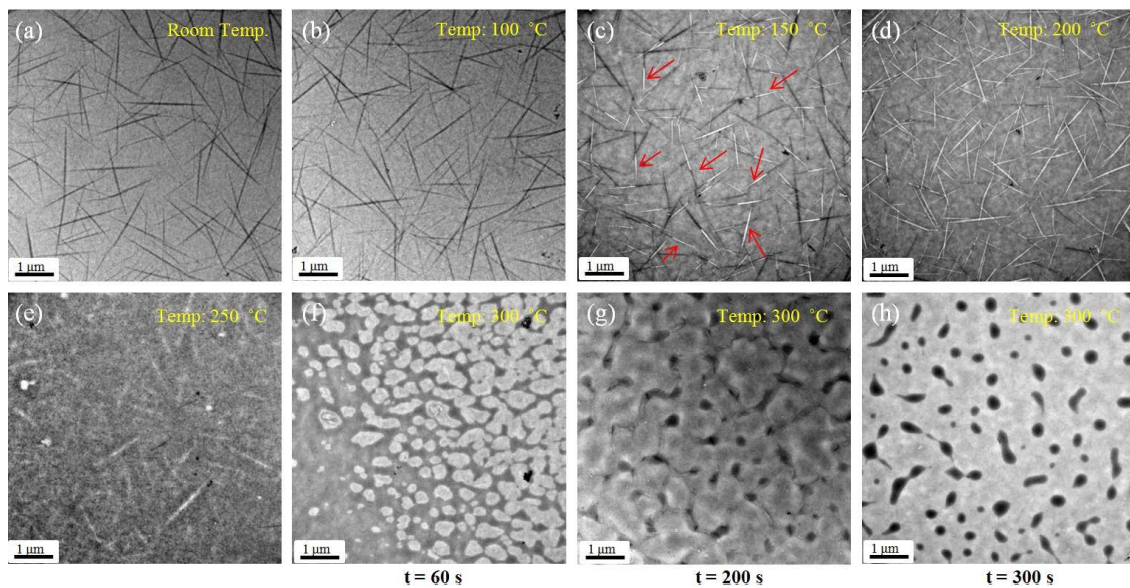




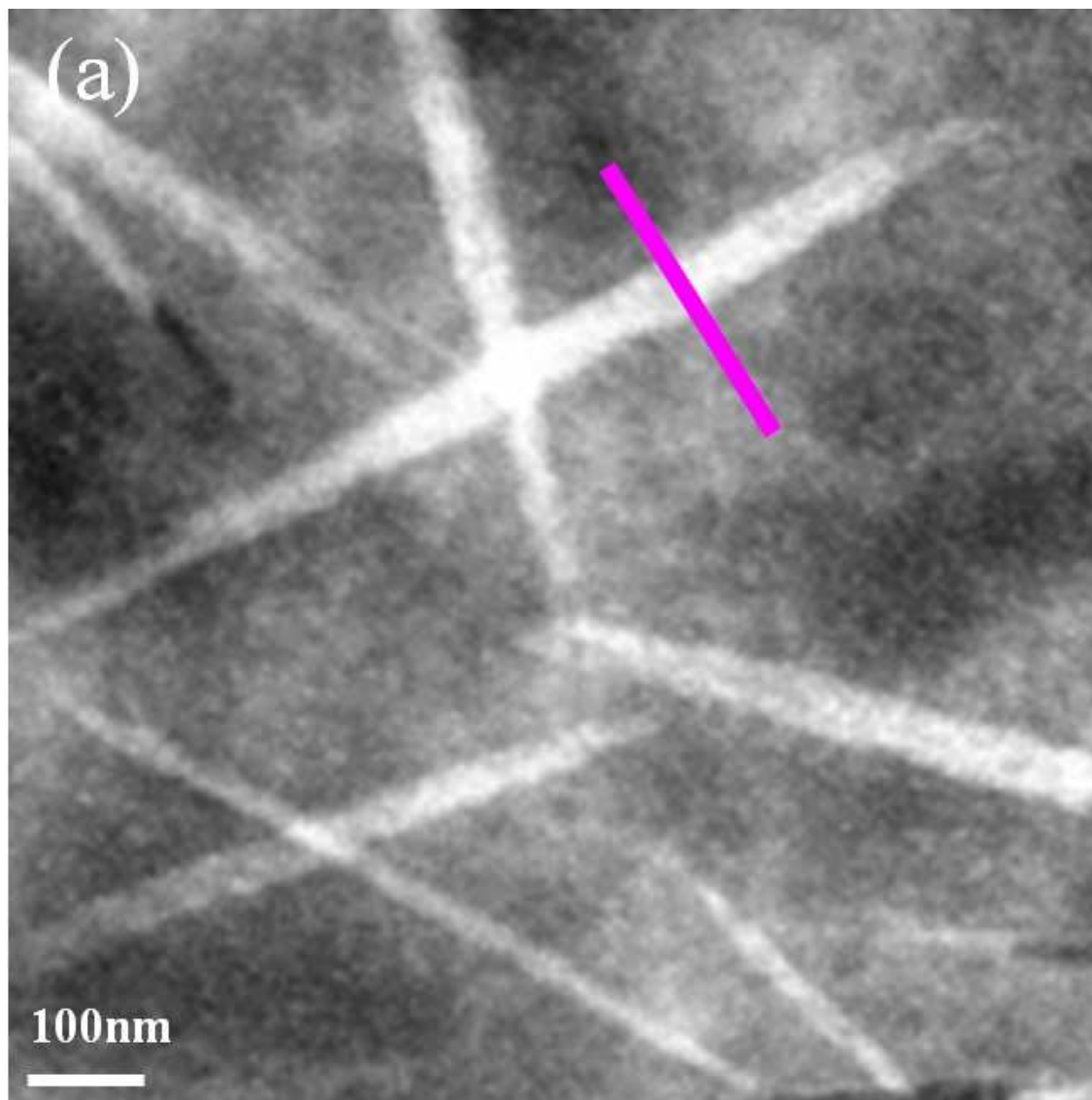
**Fig. 1.** (a) Chemical structures of the binary blend components, i.e. guest Ir(ppy)<sub>3</sub> and host PVK materials, (b) TEM image showing the stacking structure of OLED device containing PVK:Ir(ppy)<sub>3</sub> binary blend films, and (c) energy level diagram of the device fabricated in the present work.

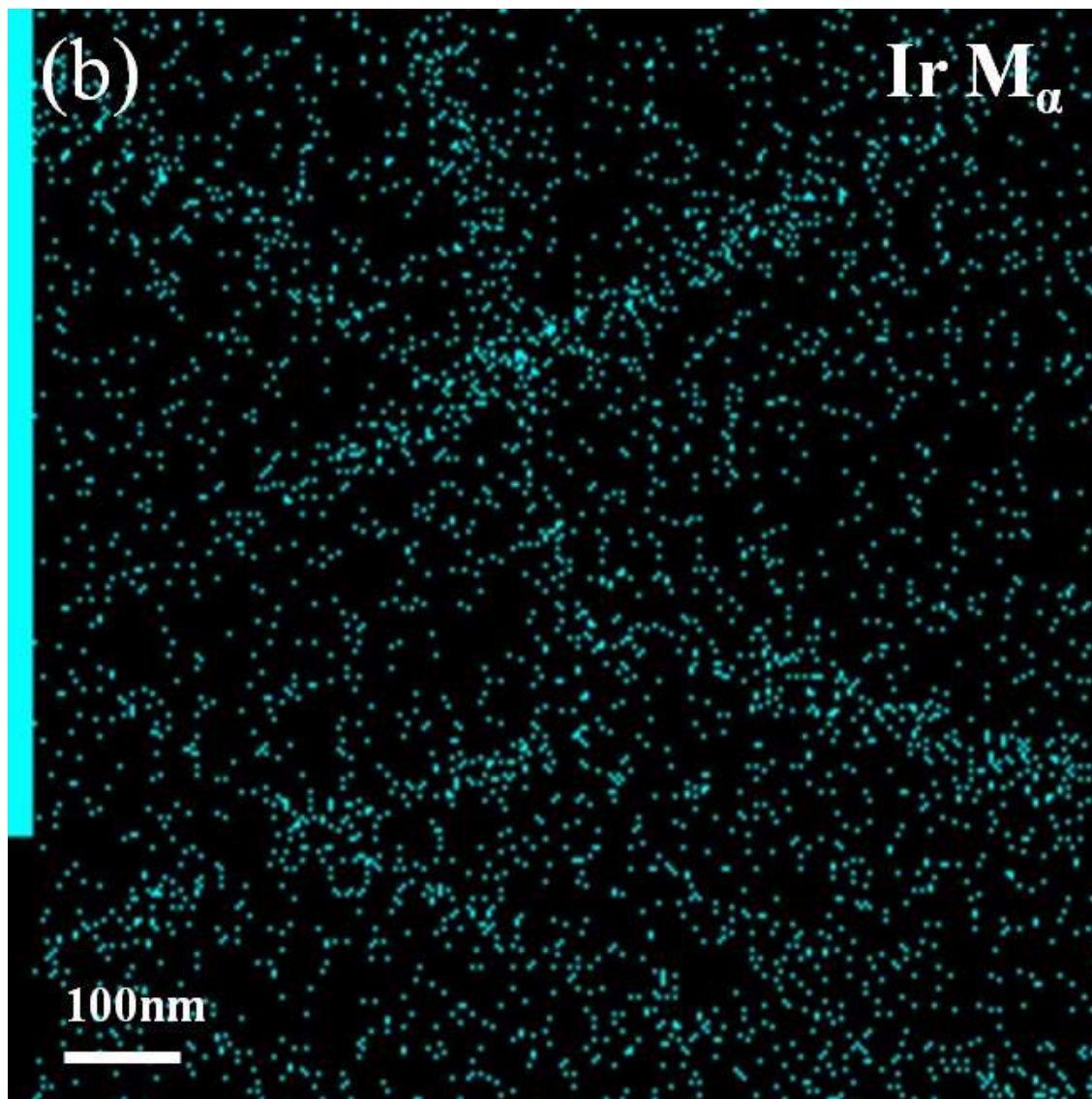


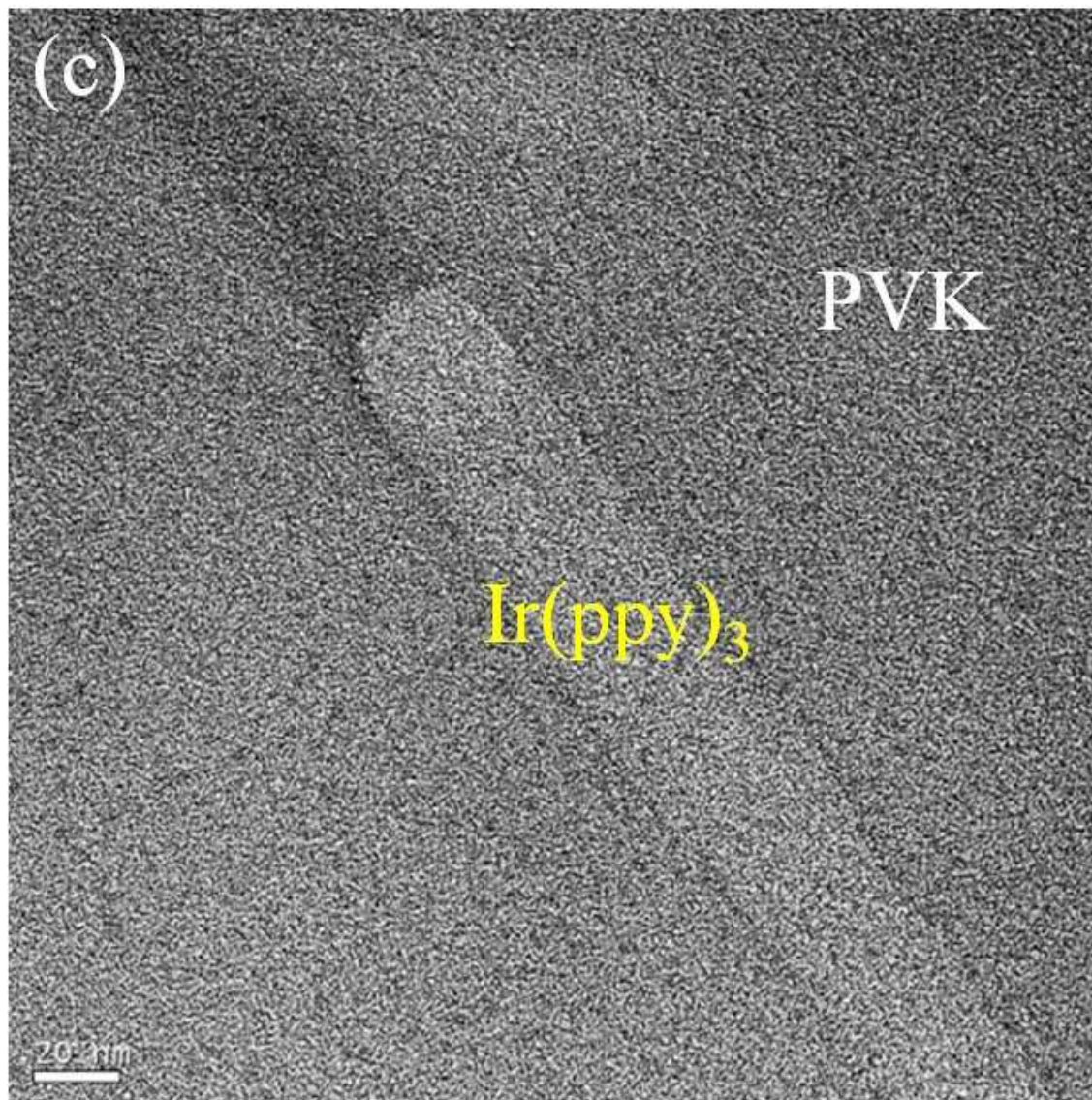
**Fig. 2.** Device performances of PVK:Ir(ppy)<sub>3</sub> films with respect to thermal annealing: (a) current density, (b) EL spectra, (c) current efficiency, and (d) luminance. The blank rectangles, circles, and triangles represent the as-processed state, annealed at 200 °C and 300 °C, respectively.

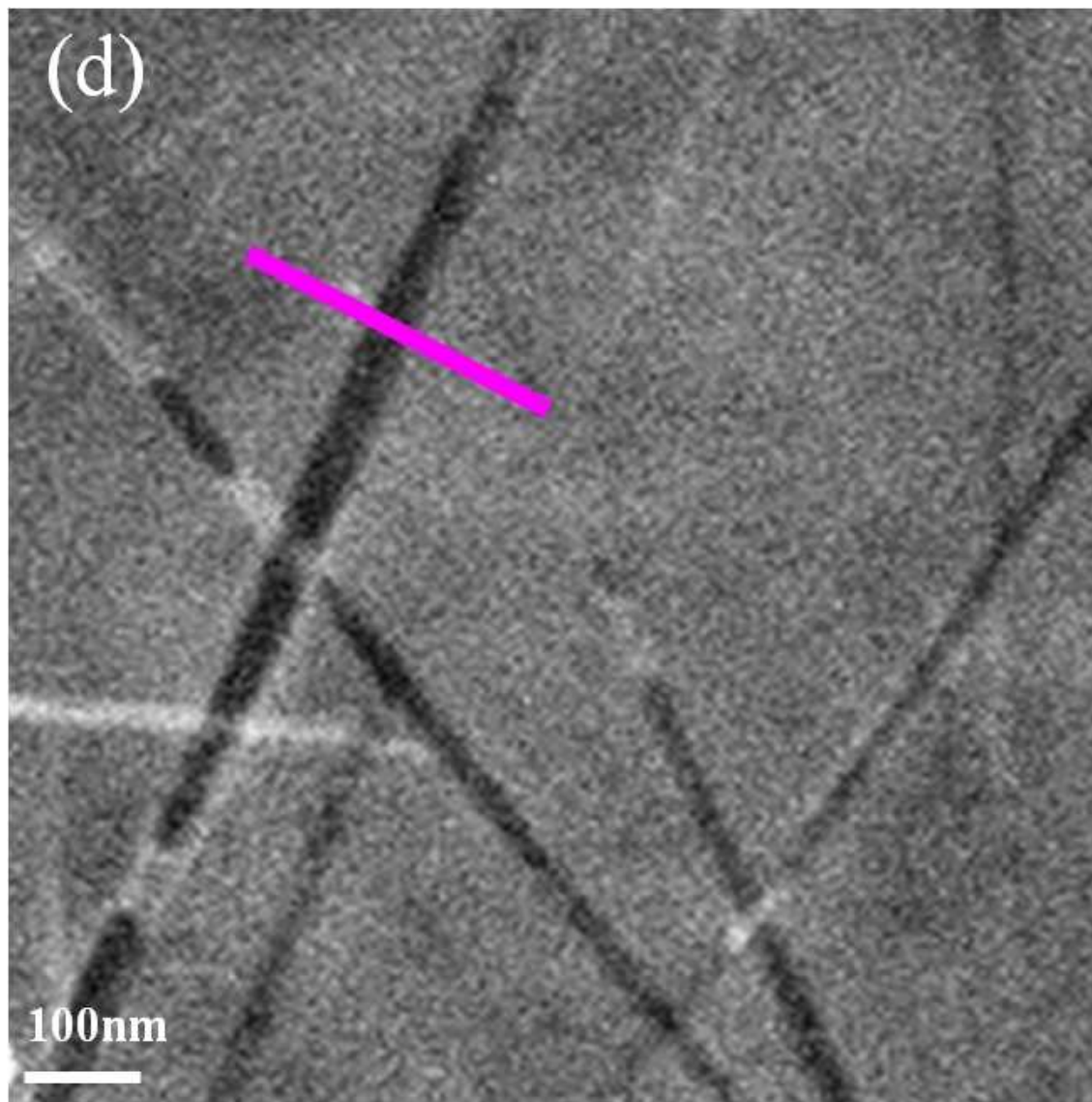


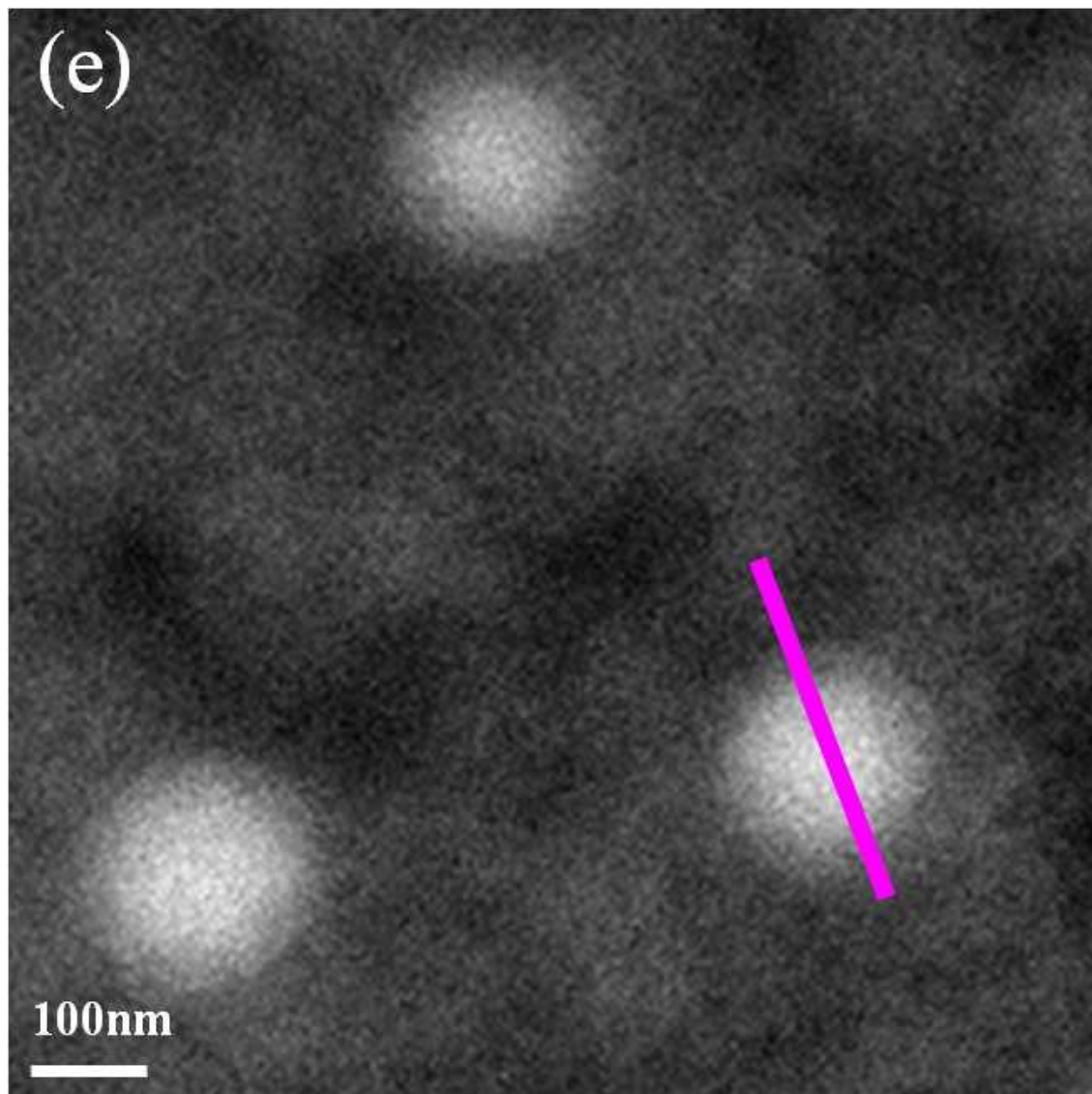
**Fig. 3.** Bright-field images observed by in-situ temperature dependent TEM experiments ranging from room temperature to 300 °C: (a) as-processed PVK:Ir(ppy)<sub>3</sub> binary blend film, (b) 100 °C, (c) 150 °C, (d) 200 °C, (e) 250 °C, and (f) 300 °C, respectively. (g) and (f) The time-dependent pattern evolution occurring at 300 °C. Note that the local contrast changes of the needle-like features are shown within the limited temperature regime as marked with the arrows.











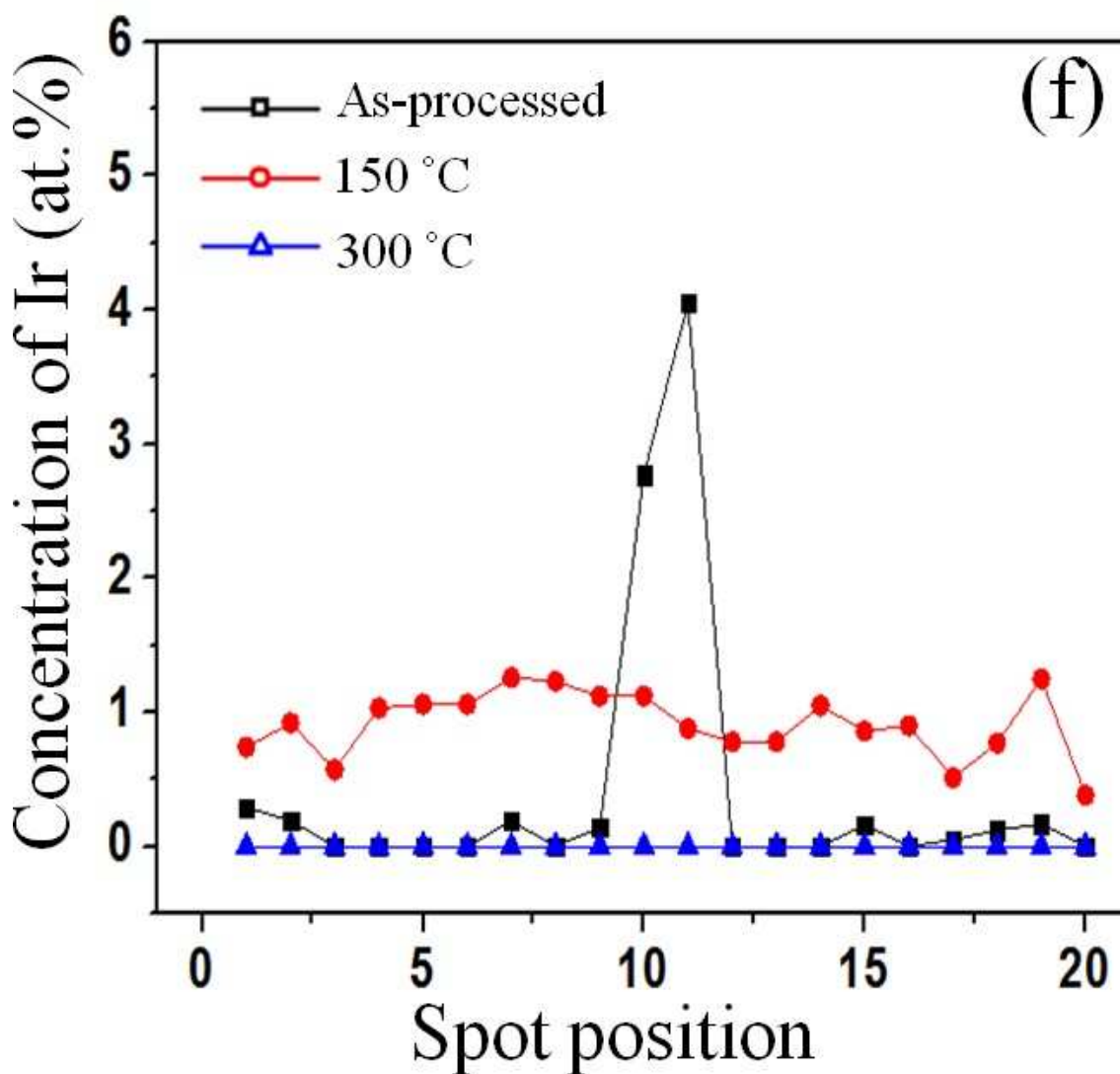
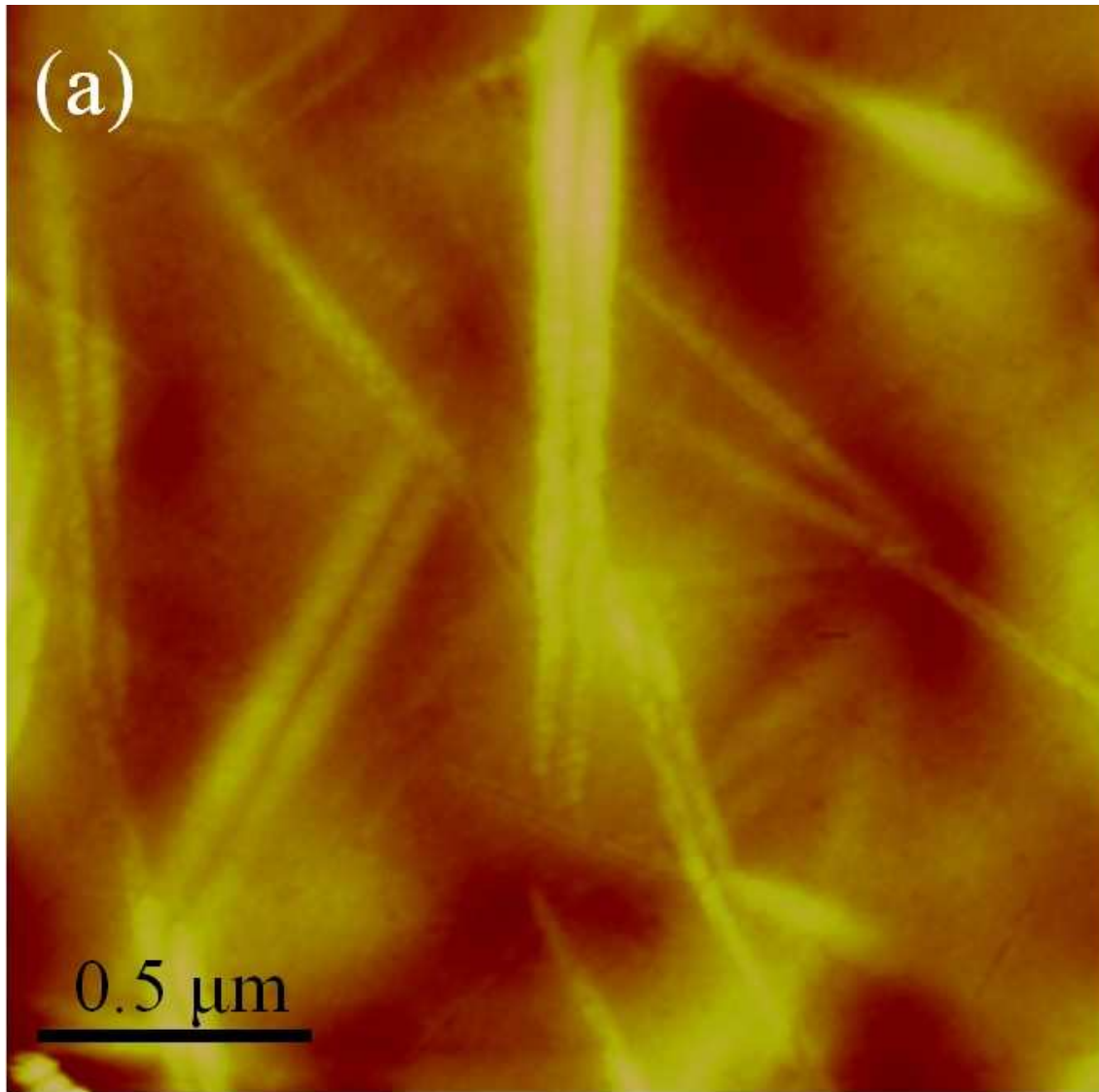
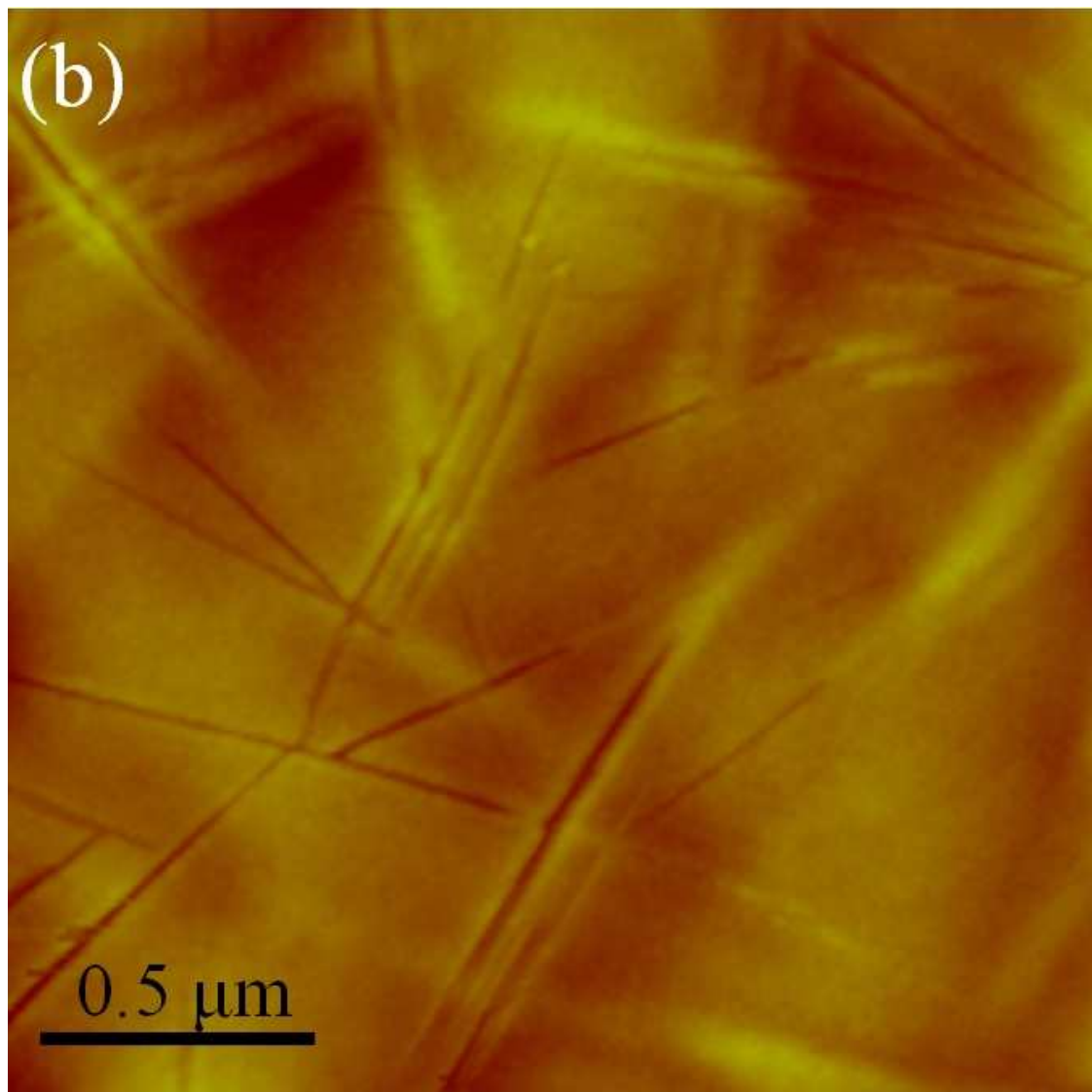


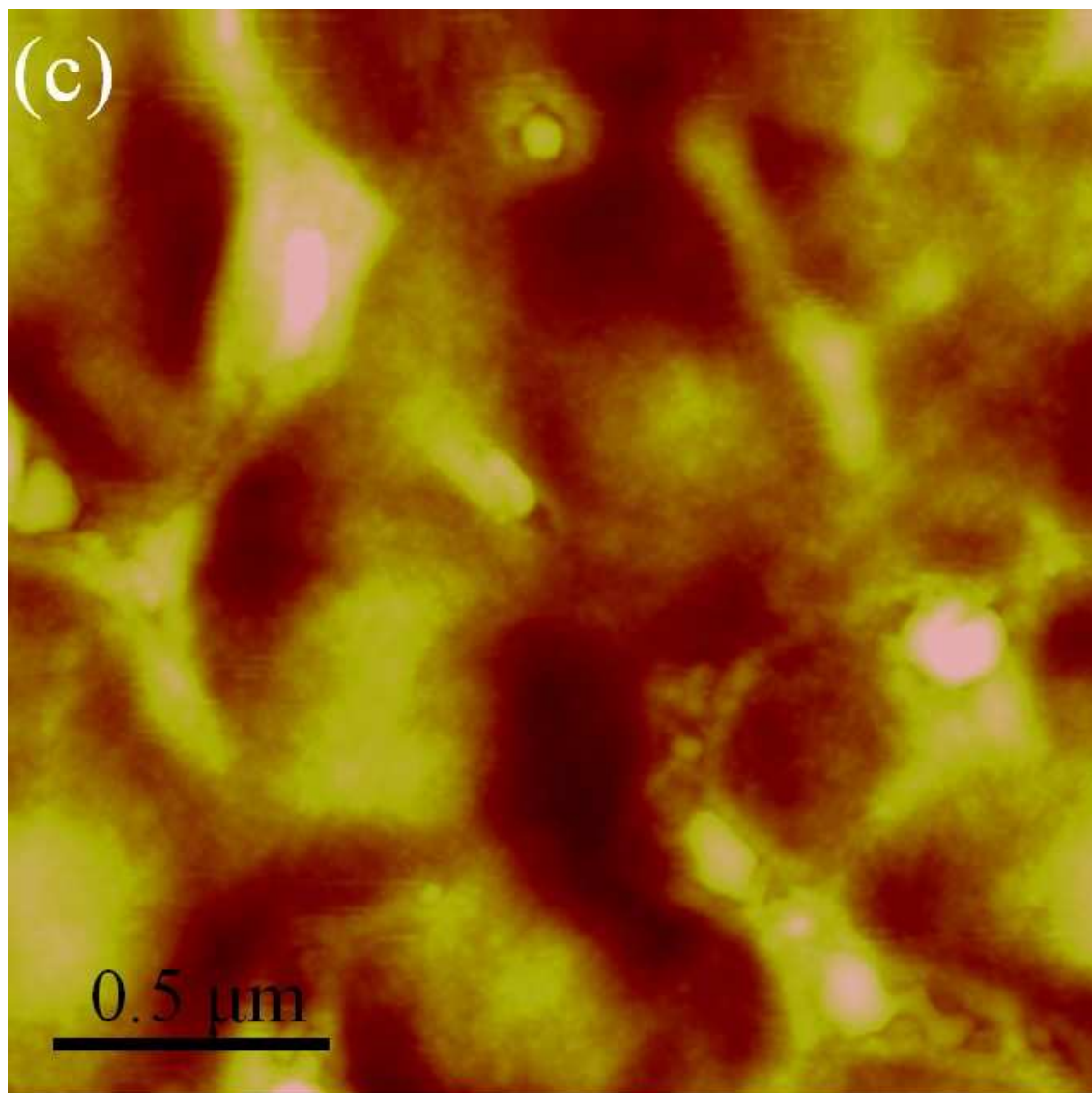
**Fig. 4.** (a) HAADF-STEM image taken from as-processed PVK:Ir(ppy)<sub>3</sub> binary blend films and (b) the corresponding enlarged EDS elemental map of Ir ( $M_{\alpha}$ ). (c) The high-resolution (S)TEM image of the film annealed at 150 °C. HAADF-STEM images of thermally annealed at (d) 150 °C and (e) 300 °C, respectively. (f) The corresponding 1-D concentration profiles of Ir along the direction (marked with the arrows taken from ROI) across the interfaces between needles and PVK. The rectangles, circles, and triangles represent the as-processed state, annealed at 150 °C and 300 °C, respectively.



RMS: 5.25nm



RMS: 2.78nm



RMS: 9.03nm

**Fig. 5.** Tapping mode AFM height images of (a) as-processed PVK:Ir(ppy)<sub>3</sub> binary blend films, and thermally annealed films at (b) 150 °C and (c) 300 °C, respectively.

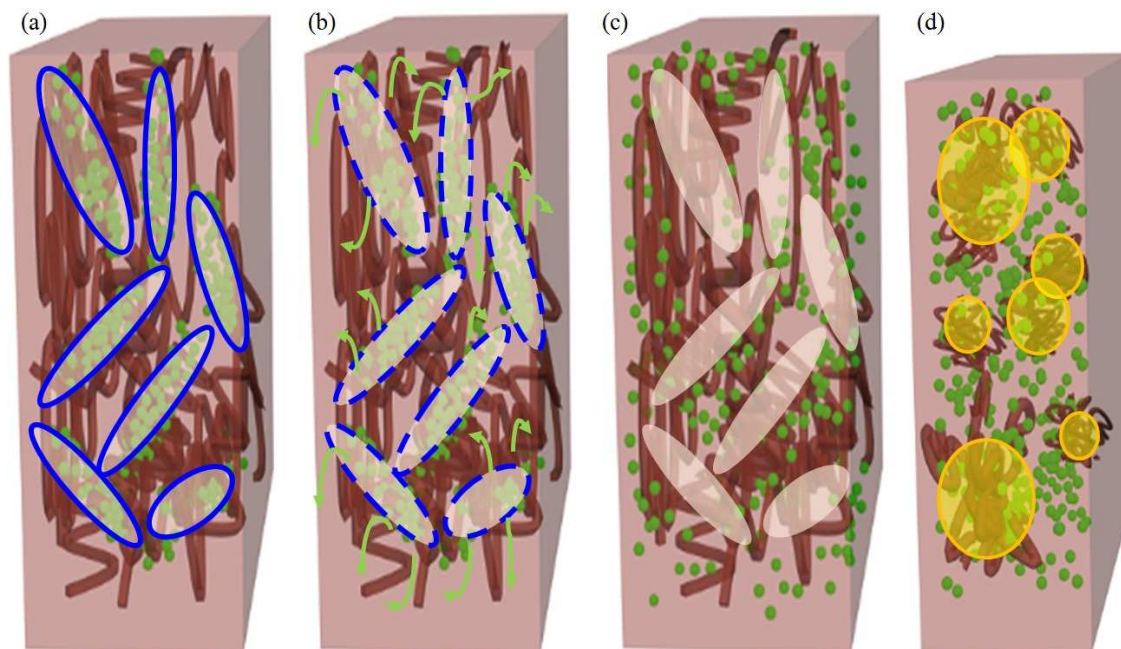


**Fig. 6.** Schematic illustrations showing the overall sequence of microstructural evolution occurring in thermally annealed PVK:Ir(ppy)<sub>3</sub> binary blend system. The green dots, blue needles, and yellow circles represent Ir(ppy)<sub>3</sub>, aggregation of Ir(ppy)<sub>3</sub> molecules, and droplet pattern of PVK, respectively. Note that at 300 °C the binary blend film shrinks, leading to a reduction of its volume.